Physica C 168 (1990) 239–248
North-Holland

SPECIAL GRAIN BOUNDARIES IN HIGH-T_c $Bi_2Sr_2CaCu_2O_{8+\delta}$

O. EIBL
Siemens Research Laboratories, Otto Hahn Ring 6, D-8000 Munich 83, FRG

Received 5 January 1990
Revised manuscript received 14 March 1990

The structure of grain boundaries of highly dense $Bi_2Sr_2CaCu_2O_{8+\delta}$ was investigated by high-resolution transmission electron microscopy. Special grain boundaries were observed for which the *c*-axes of adjacent grains were parallel to each other. Grains which are rotated with respect to each other by approximately 45° around the *c*-axis form coherent (001) grain boundaries. For (001) twin boundaries the rotation angle is 90° around the *c*-axis. For coherent (001) grain boundaries and twin boundaries, the interfaces lie between two adjacent (001) BiO layers. This indicates that the formation of (001) interfaces between these two layers is energetically most favourable due to the large bond lengths resulting in weak chemical bonds. Polytypoids, i.e. lamellae of $Bi_2Sr_2Ca_{n-1}Cu_nO_{4+2n+\delta}$ phases with $n \neq 2$, are frequently observed at twin boundaries and also occur at small angle tilt boundaries to accommodate for the mismatch. This yields compositional variations along the boundary. The dislocations in the boundary introduce either additional perovskite layers or Bi–O double layers. The latter dislocations occur less frequently and convert one lamella with $n=3$ or $n=4$ into two lamellae of $n=1$ phase. Incoherent grain boundaries show no evidence of intergranular phases. Thus, the weak-link behaviour of grain boundaries, which is observed in $YBa_2Cu_3O_{7-x}$ might not occur in $Bi_2Sr_2CaCu_2O_{8+\delta}$ ceramics.

1. Introduction

Recently, Maeda et al. [1] found high-T_c compounds in the $Bi_2Sr_2Ca_{n+1}Cu_nO_{4+2n+\delta}$ system. Different phases exist in this system which can be characterized by the number of CuO planes parallel to the (001) crystallographic planes. The crystal structure of these phases consists of Bi–O double layers and perovskite-type cuboids containing Sr, Ca, Cu and O sandwiched between the Bi–O double layers. Depending on the number of CuO planes in the (half) unit cell we refer to the $n=1$ phase ($c=2.46$ nm), the $n=2$ phase ($c=3.09$ nm, $T_c \approx 80$ K) and the $n=3$ phase ($n=3.7$ nm, $T_c \approx 110$ K). These phases have one-dimensional incommensurate modulations with wave vectors $q=b^*/4.7$. For the $n=2$ and $n=3$ phases the incommensurate component of the wave vector is parallel to one of the short crystal axes. Besides the analysis of the crystal structure, the microstructure of these compounds is interesting both from the crystallographic and technological point of view. Formation of polytypoids is frequently found in material which contains the $n=3$ phase as the majority phase. Intergrown lamellae share common (001) planes and a stacking fault density of up to 10^9/m can be observed. In resistivity versus temperature curves, intergrowth results in two drops of the resistivity and the resistivity reaches zero only below T_c of the $n=2$ phase.

Besides the $n=3$ phase, the $n=2$ phase also has a T_c well above 77 K. Therefore, this phase is of considerable technological interest. When it is carefully prepared in a mixed-oxide preparation process, planar defect densities can be as low as 10^6/m within the grains. For technological application of this material the influence of crystal defects, especially grain boundaries, on its electrical properties is of great interest.

When an external magnetic field (between H_{c1} and H_{c2}) is applied, the field penetrates into the bulk of a type II superconductor in the form of quantized flux vortices [2]. When an electrical current flows through the sample, a Lorentz force acts on the vortices and results in energy dissipation unless the vortices are pinned. Defects, particularly interfaces, play a significant role in the extremely high critical cur-

rent densities which can be achieved in type II superconducting oxides.

While grain boundaries will interact with flux vortices and raise critical densities, they also may act as weak links in the conduction path resulting in poor intergrain coupling in the superconducting state. Depending on the behaviour of j_c with temperature and external magnetic fields, one distinguishes superconducting grains separated by either metallic or insulating layers. For the high-T_c compound $YBa_2Cu_3O_{7-x}$ it was recognized that grain boundaries determine the electrical properties of bulk ceramics in the superconducting state. Also, by the lack of a proper control of the grain boundary structure, electrical properties of $YBa_2Cu_3O_{7-x}$ ceramics are inferior when compared to single crystals and single crystalline thin films. Thus, understanding of grain boundary properties in the new high-T_c superconducting oxides will be the key for increasing critical currents especially under high magnetic fields and temperatures well above 4 K.

1.1. Crystal structure of $Bi_2Sr_2CaCu_2O_{8+\delta}$

The crystal structure of $Bi_2Sr_2CaCu_2O_8$ consists of BiO layers and oxygen deficient perovskite-like cuboids containing Sr, Ca, Cu and O. This is best explained by looking at the average structure described by space group Pccn (fig. 1). The real structure of this phase differs significantly from that shown in fig. 1, due to an incommensurate modulation parallel to the b-axis. The displacive part of the modulation can be observed in high-resolution images in the [100] pole. The displacement fields is two-dimensional, i.e. the displacement of atoms with respect to the basic structure parallel to the x-axis is very small. The modulated crystal structure can be understood in terms of a basic structure belonging to one of the 230 space groups and superimposed, periodic structural distortions with amplitudes of approximately 40 pm in the b-direction and 10 pm in the c-direction. A structural model for the cation sublattice was proposed in ref. [3] and contains four displacement waves (two for Bi, one for Sr and one for Cu). Amplitudes and phases of these displacive waves were given in ref. [3]. The incommensurate modulations have wave vectors $q=b^*/4.7=(2.6\ \text{nm})^{-1}$.

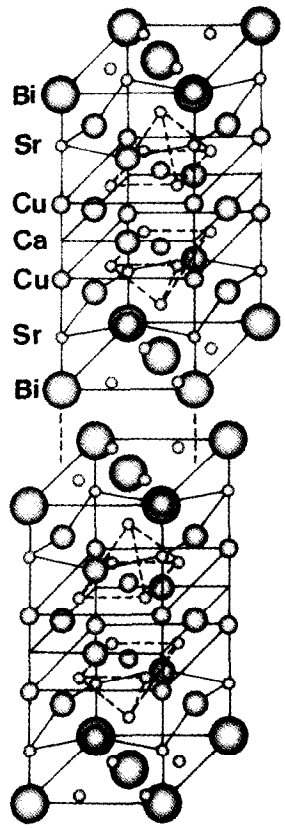

Fig. 1. A unit cell of the average structure of $Bi_2Sr_2CaCu_2O_{8+\delta}$. Cations are indicated by the symbol of the element in one half of the unit cell and small circles indicate oxygen atoms.

In this paper we introduce a crystal lattice with lattice parameters $a \approx b = 0.54$ nm and $c = 3.09$ nm. The wave vector of the modulation is parallel to the b-axis.

2. Experimental

Preparation of $Bi_2Sr_2CaCu_2O_{8+\delta}$ samples was explained in detail in ref. [4]. Te nominal cation composition of the samples was $Bi_2Sr_2CaCu_2$. Oxide powders were milled, mixed and finally compacted. The powder mixture was melted in Al_2O_3 crucibles at 1050°C for 15 min. The melt was cast into a thin walled Cu mould ($25\times25\times50$ mm^3). The temperature was then rapidly dropped to about 600°C and

the material was cooled to room temperature in about one hour. After this, the material consisted of the $n=1$ phase $Bi_2(Sr_{1-x}, Ca_x)CuO_{6+\delta}$ ($x<0.33$) and earth alkali cuprates. This heterogenous system was then transformed into the desired 2212 phase by an annealing at approximately 815°C for 20 to 200 h. The melting and decomposition temperature is known to be 890°C.

This preparation procedure leads to *high-density* (>90% of the theoretical density) ceramics with $T_c=86$ K and is of considerable technological interest.

Disks, 3 mm in diameter, were cut and TEM specimens were prepared by grinding, dimpling and finally ion milling with effective liquid nitrogen cooling. TEM samples were studied in a 400 kV microscope equipped with a high-resolution pole piece (0.18 nm point-to-point resolution). All images shown in this paper were obtained at the vary thin edge of the specimens. In the thinnest region of the image thickness was estimated to be 2–3 nm. Imaging conditions were at or very close to Scherzer defocus. This was confirmed by taking optical diffractograms of the high-resolution images. They did not show any detectable astigmatism for any of the images presented here. As a consequence black dots can be interpreted as atomic columns of heavy elements, i.e. Bi, Sr, Cu and Ca. White dots correspond to atomic columns of light elements, i.e. O or vacancies.

In this paper we present results on the structure of special grain boundaries in $Bi_2Sr_2CaCu_2O_{8+\delta}$. These grain boundaries separate grains with a special orientation relationship between each other.

3. Results and discussion

3.1. Twin boundaries

In this structure twin boundaries result when one part of the crystal is rotated by 90° with respect to the other around the common [001] axis. These twins are growth twins and should not be confused with deformation twins which are found in, e.g., $YBa_2Cu_3O_{7-x}$. A twin boundary is shown in fig. 2. In the upper part the beam direction is parallel to the [100] axis and in the lower part to [010]. Atomic columns containing Bi atoms are indicated by ar-

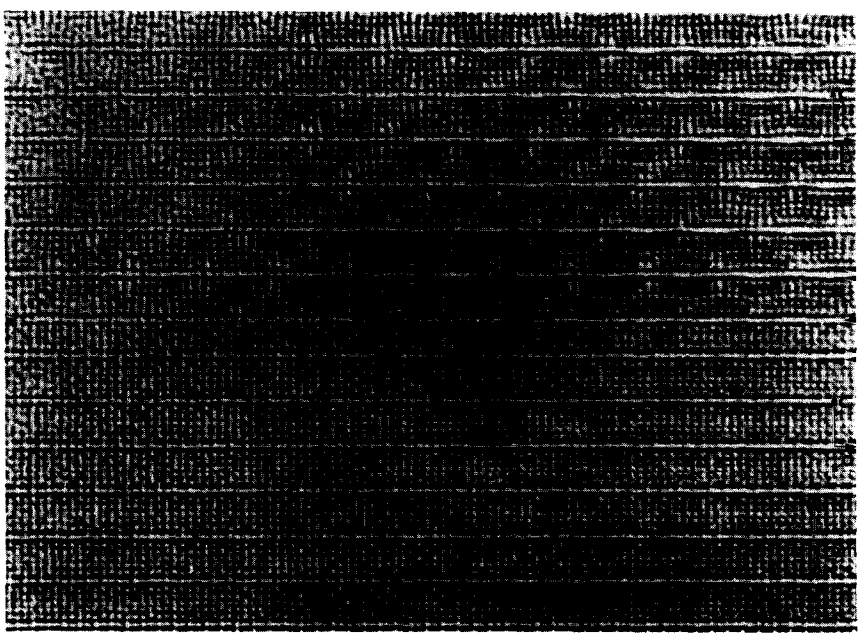

Fig. 2. Twin boundary in $Bi_2Sr_2CaCu_2O_{8+\delta}$. The electron beam is parallel to the [100] and [010] directions of matrix and twin, respectively. The boundary is indicated by single arrows. Bi atomic columns in Bi–O double layers are also indicated by arrows.

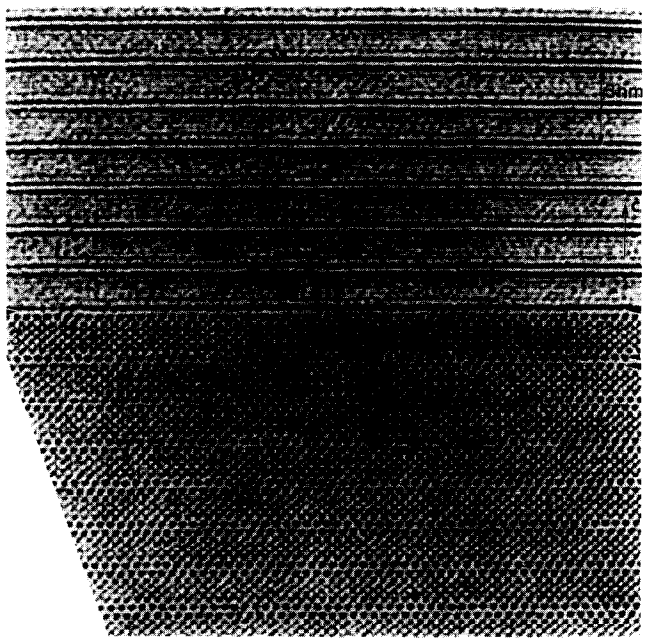

Fig. 3. Twin boundary in $Bi_2Sr_2CaCu_2O_{8+\delta}$. The electron beam is parallel to the [110] pole only in the lower part of the bicrystal.

rows and appear as black dots. At the twin boundary an intrinsic stacking fault is formed which introduces a lamella of the $n=1$ phase. The wavy contrast in the upper part of the crystal results from a (displacive) modulation described in more detail in ref. [3]. The twin boundary passes between two neighbouring Bi–O double layers as is indicated by single arrows. One layer at the boundary belongs to the [100] orientation and shows a wavy contrast and the other Bi–O layer shows the contrast of the [010] orientation. In this orientation Bi atomic columns appear in pairs and do not lie equidistantly along the [100] direction. This is due to the shift of Bi atoms from special positions in the Fmmm space group. Finally, the contrast changes due to different foil thicknesses are apparently stronger in the [100] orientation compared to the [010] orientation.

When twin boundaries are imaged in the [110] pole only one part of the bicrystal can be oriented in such a way that the beam direction is parallel to the zone axis (fig. 3). The second part deviates slightly ($\approx 0.02°$) from the proper orientation since the lattice parameter ratio deviates from unity: $b/a=1.001$. The effect of the really small misalignment on the image contrast is rather strong. Due to the misalignment Bi atomic columns are no longer parallel to the beam but overlap in projection, resulting in a dark line. The [110] projection is valuable to find the exact location of the twin boundary. At the boundary one line of dark dots is observed in the lower part of the bicrystal and a uniform dark line in the upper part. The twin boundary is located between the Bi–O atomic layers. At this twin boundary a lamella of the $n=3$ phase is present.

3.2. Grain boundaries

Besides twin boundaries, special grain boundaries were observed for which both gains had parallel (001) planes. The grain boundary in fig. 4 lies on a (001) plane and separates two grains which are misoriented by a rotation of approximately 45° about the common c-axis. In the upper grain the beam direction is parallel to the [100] pole and in the lower grain close to [110]. The amount of deviation from the exact [110] orientation is similar to the upper crystallite of fig. 3. The grain boundary is indicated by arrows and passes also between two Bi–O layers

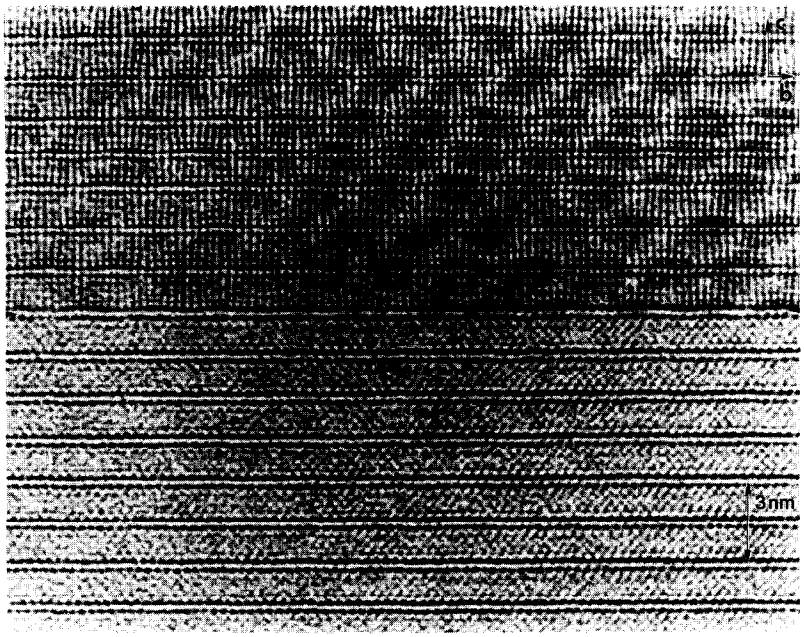

Fig. 4. Grain boundary in $Bi_2Sr_2CaCu_2O_{8+\delta}$. (001) lattice planes are parallel in the two crystallites. The interface is indicated by arrows.

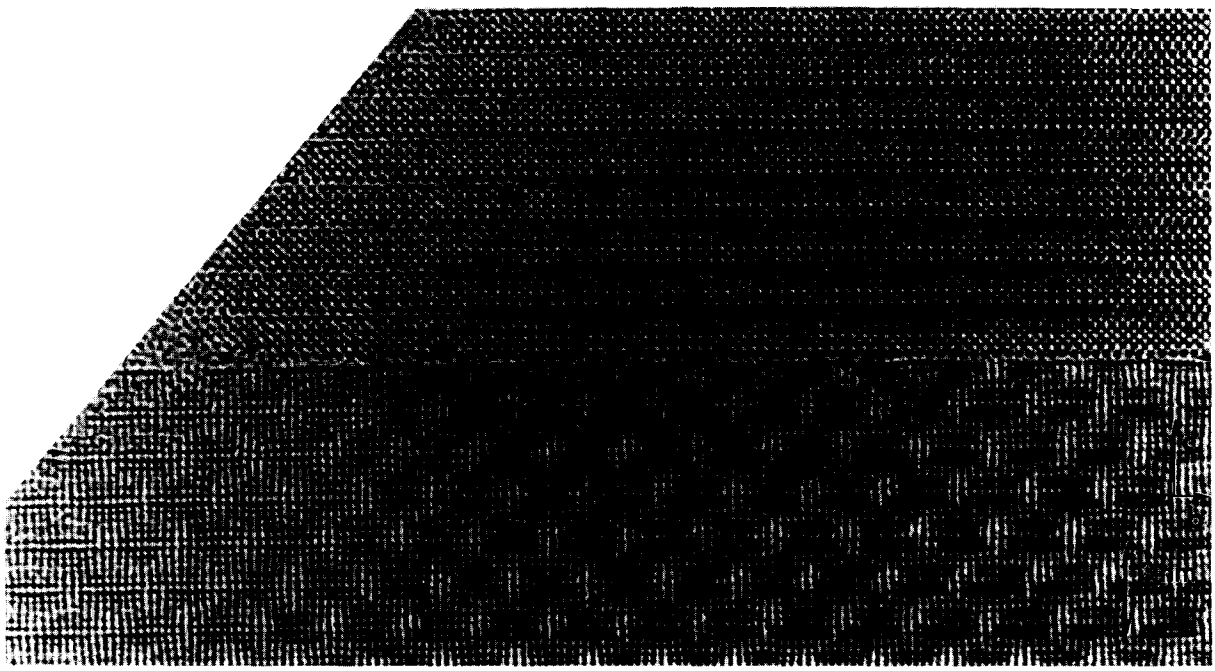

Fig. 5. Grain boundary in $Bi_2Sr_2CaCu_2O_{8+\delta}$. (001) lattice planes are rotated by 1° along an axis in the plane of the interface (tilt component).

of the crystal structure: one Bi–O layer belongs to the grain in the [100] orientation and shows a wavy contrast, while the other Bi–O layer belongs to the grain for which the beam direction is almost parallel to the [110] direction.

At a distance of one unit cell above the grain boundary a stacking fault ($n=1$) is observed which introduces a lamella of the $n=1$ phase. At the boundary, however, no polytypoids are found.

Another example of a special grain boundary is

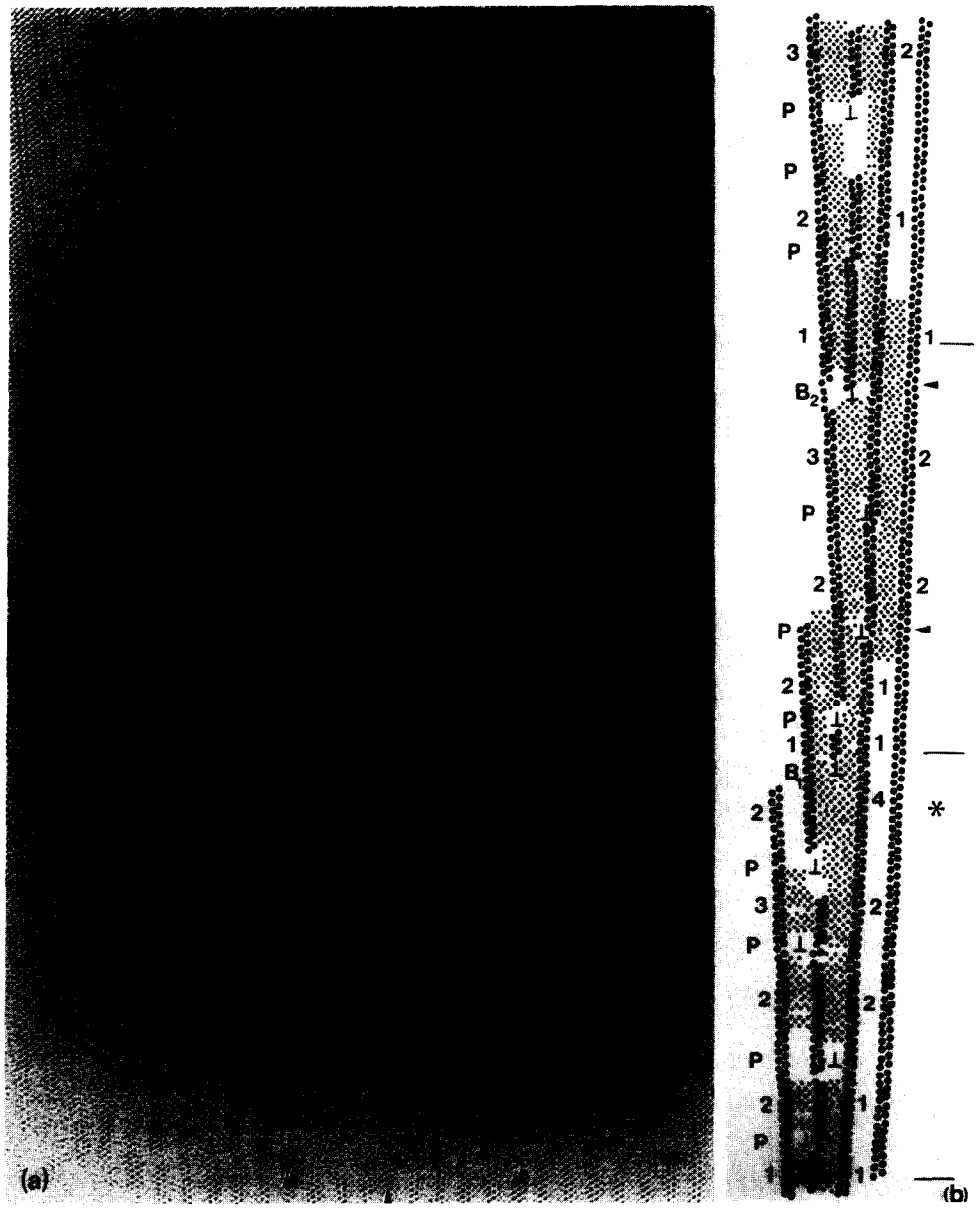

Fig. 6. (a) Small-angle (4°) tilt boundary in $Bi_2Sr_2CaCu_2O_{8+\delta}$. (b) Schematic reconstruction of the 4° tilt boundary. Large circles indicate Bi atoms in Bi–O double layers and small circles indicate atoms in the perovskite-like blocks, i.e. Sr, Ca and Cu. This section of the grain boundary contains a step indicated by arrows. The periodicity in the structure of the boundary is indicated.

shown in fig. 5. This boundary separates two grains which have a similar orientation relationship as in fig. 4. However, in this case the beam direction is exactly parallel to the [100] and [110] directions, respectively. The two grains are rotated by approximately one degree about an axis lying parallel to the beam direction and therefore introducing a small tilt component. At the boundary the single line of black dots shows up clearly from the upper crystallite with [110] orientation.

In the left part of the image one Bi–O plane in [110] orientation and one in [100] orientation can be observed enclosing an angle of 1 degree. The distance between these planes is 0.6 nm in the very left part of the image. The structure between the two Bi–O planes at the boundary is not clear and might have been changed by the ion milling process. In the middle of the image the distance between the Bi–O layers of different orientation reaches its intrinsic value of 0.31 nm. In the right part of the image the contrast becomes complicated due to dynamical effects and an interpretation is not possible without detailed image simulation.

A small angle ($\approx 4°$) tilt boundary is shown in fig. 6(a). The homogenous contrast along a rather long distance (≈ 70 nm) of the boundary is remarkable and allows the atomic positions to be constructed. In the schematic drawing (fig. 6(b)) it becomes clear that polytypoids are formed to accommodate for the mismatch due to the 4° misorientation. The insertion of additional perovskite-like blocks is observed to occur within one unit cell at the grain boundary. The number of perovskite-like blocks inserted between Bi–O double layers increases when going from bottom to top: the structure starts with a unit cell of the $n=1$ phase and the second half of the unit cell which is further away from the boundary is enlarged first (parallel to the c-direction). To explain the

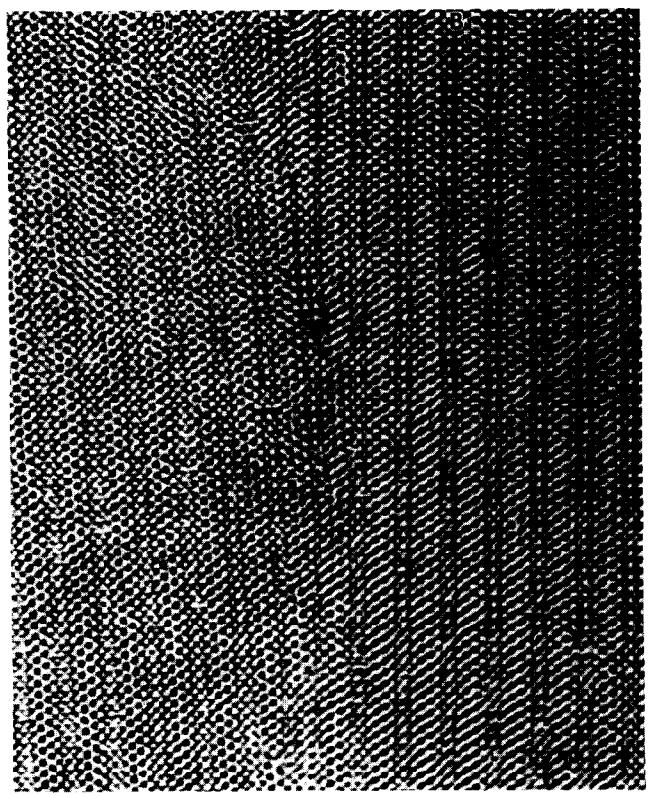

Fig. 7. About one period of the grain boundary of fig. 6.

Fig. 8. Large-angle grain boundary in $Bi_2Sr_2CaCu_2O_{8+\delta}$. The boundary is indicated by arrows. Bi atomic columns in Bi–O double layers are indicated.

structure at the boundary we use the notation $x:y$, in which x denotes the phase ($n=1, 2, 3...$) in the second half unit cell and y th first half unit cell at the boundary. The sequence then is 1:1, 2:1, 2:2, 3:2, ..., 1:1, etc., which means a periodic arrangement of polytypoids at the boundary. Looking at the schematic drawing one can find two steps (indicated by arrows) at the grain boundary lying approximately 10 nm apart. Insertion of additional layers results in two different types of partial dislocations at the low angle tilt boundary: (i) dislocations which allow an insertion of Bi–O double layers (type 1, "B" in fig. 6(b)) and (ii) dislocations which allow an insertion of an additional layer of perovskite-like cuboids (type 2, "P" in fig. 6(b)). Type 1 dislocations convert one $n=4$ or $n=3$ lamella into *two* $n=1$ lamellae. The Burgers vector components parallel to the c-axis then are 0.3 nm ("B_1") and 0.5 nm ("B_2"), respectively. Type 2 dislocations convert a $n=n_0$ lamella into a lamella with $n=n_0+1$, and the component of the Burgers vector parallel to the c-axis is approximately 0.3 nm. About one period of the polytypoid arrangement along the boundary is shown in larger magnification (fig. 7). These high-resolution images (figs. 6 and 7) indicate that perovskite blocks appear to be strained up to 10% and therefore help to accommodate for the mismatch.

Special boundaries were frequently observed in the ceramic samples, although there was no indication of texture by X-ray diffraction analysis. Besides boundaries with a special orientation relationship, i.e. coincide of low index crystallographic directions, large angle grain boundaries are also present. In the image of fig. 8 the c-axes of both grains forming the grain boundary are coplanar enclosing an angle of 31° and lie in the plane of projection. Thus, Bi–O layers are observed in both grains. In the lower grain the beam direction is parallel to a [100] direction and the displacive modulation yields a wavy lattice fringe contrast. At the grain boundary (indicated by arrows) no intermediate layer is observed.

4. Conclusions

4.1. Structural properties

Special grain boundaries are observed in $Bi_2Sr_2CaCu_2O_{8+\delta}$ ceramics. They are formed between grains for which the c-axes are parallel to each other. Among the observed boundaries, for which the adjacent grains have parallel c-axes, in certain cases additional low index directions of the two grains were parallel. These boundaries separate grains which are rotated with respect to each other by approximately 45° around the c-axis and the [100] direction of one grain was parallel to the [110] direction of the other.

These boundaries can be clearly distinguished from twin boundaries which result by a rotation of 90° around the *c*-axis.

Grain boundaries lie frequency on (001) planes of one of the two crystallites if small tilt components occur. When interfaces are formed on (001) planes, i.e. for special grain boundaries and twin boundaries, interfaces always lie *between* two adjacent (001) Bi–O layers which together form the Bi–O double layer. Thus the formation of an interface is energetically more favourable between two Bi–O layers. Bi–O (001) layers are particular layers in $Bi_2Sr_2Ca_nCu_{n+1}O_z$ phases: (i) when material is cleaved the (001) cleavage plane lies between the Bi–O double layers [5], and (ii) the displacements due to the presence of the modulation are largest in these two layers (e.g. ref. [3]). The bonding lengths between these two layers are larger than 0.29 nm. This indicates that chemical bonds between the two Bi–O layers are weak, i.e. the bonding might be understood as a van der Waals bonding rather than ionic, making stacking fault energies, twin energies and grain boundary energies small.

At twin boundaries polytypoids are frequently observed which introduce a lamella of $Bi_2Sr_2Ca_{n-1}Cu_nO_z$ with a different *n* compared to the matrix. This indicates that a mechanism exists which makes it energetically more favourable to form the twin boundary at the stacking fault plane and vice versa. A more detailed description of the interaction of stacking faults with twin boundaries will be presented in another paper [6].

For a 4° tilt boundary with an interface parallel to a (001) plane, polytypoids were observed which accommodate for the mismatch. Since polytypoids have different chemical composition, the composition is modulated at the tilt boundary and the periodicity is determined by the misorientation of the two grains. The structure at the boundary can be described by introducing grain boundary dislocations of the edge type which have Burgers vectors equal to [100] lattice vectors of the perovskite sublattice. However, once in every periodic unit a type 1 dislocation (introducing a Bi–O double layer) has to be inserted which converts one $n=4$ or $n=3$ lamella into two $n=1$ lamellae. The components of the Burgers vectors along the *c*-axis of these dislocations are then 0.3 nm and 0.5 nm, respectively.

4.2. Electrical properties

Electrical properties of grain boundaries in $Bi_2Sr_2CaCu_2O_z$ ceramics are expected to be significantly different compared to $YBa_2Cu_3O_{7-x}$ ceramics prepared by a conventional mixed-oxide process. In $YBa_2Cu_3O_{7-x}$ second phases and high densities of extended defects are formed at grain boundaries yielding grain boundary zones approximately 100 nm to 1 μm in thickness. Critical currents show a drop of two orders of magnitude when small magnetic fields (< 1 T) are applied. It is assumed that this behaviour is determined by the presence of the grain boundary zones which act as weak links in the superconducting state.

Grain boundaries in $Bi_2Sr_2CaCu_2O_{8+\delta}$ ceramics prepared as described above show a very different microstructure at the grain boundaries. The fraction of special boundaries lying parallel to (001) planes is considerably large and these boundaries are structurally coherent. But also at structurally incoherent boundaries, no intermediate phases or defects generated at the boundary and extending perpendicularly to the boundary were observed. Thus, our results indicate that under suitable preparation conditions the weak-link behaviour of grain boundaries, which is observed in $YBa_2Cu_3O_z$ ceramics, might not appear in $Bi_2Sr_2CaCu_2O_{8+\delta}$ ceramics.

However, for technological application grain boundaries and other extended crystal defects must be introduced as pinning centers in order to achieve high critical currents. In particular, extended crystal defects have to be found as pinning centers which can prevent thermally activated flux creep in this material.

Acknowledgements

The author is indebted to E. Preisler and J. Bock (Hoechst) for providing carefully prepared samples, to the Federal Department of Research and Technology (BMFT) for financial support and to H. Oppolzer for reading the manuscript.

References

[1] H. Maeda, Y. Tanaka, M. Fukutomi and T. Asano, Jpn. J. Appl. Phys. 27 (1988) L209.
[2] A.A. Abrikosov; Sov. Phys. JETP 5 (1957) 1174.
[3] O. Eibl, Physica C 168 (1990) 215 (this issue).
[4] J. Bock and E. Preisler, Proc. MRS Spring Meeting, San Diego, April 1989.
[5] Y. Matsui, H. Maeda, Y. Tanaka and S. Horiuchi, Jpn. J. Appl. Phys. 28 (1989) L946.
[6] O. Eibl, Physica C 168 (1990) 249 (this issue).